Thermal combination therapies for local drug delivery by magnetic resonance-guided high-intensity focused ultrasound

Nicole Hijnen[a,1], Esther Kneepkens[a,1], Mariska de Smet[a], Sander Langereis[b], Edwin Heijman[b,c], and Holger Grüll[a,c,2]

[a]Department of Biomedical Engineering, Biomedical NMR, Eindhoven University of Technology, Eindhoven, 5600 MB Eindhoven, The Netherlands; [b]Department of Oncology Solutions, Philips Research Eindhoven, 5656 AE Eindhoven, The Netherlands; and [c]Department of Radiology, Experimental Imaging and Image-Guided Therapy, University Hospital of Cologne, 50937 Cologne, Germany

Edited by Robert Langer, Massachusetts Institute of Technology, Cambridge, MA, and approved April 25, 2017 (received for review January 15, 2017)

Several thermal-therapy strategies such as thermal ablation, hyperthermia-triggered drug delivery from temperature-sensitive liposomes (TSLs), and combinations of the above were investigated in a rhabdomyosarcoma rat tumor model (n = 113). Magnetic resonance-guided high-intensity focused ultrasound (MR-HIFU) was used as a noninvasive heating device with precise temperature control for image-guided drug delivery. For the latter, TSLs were prepared, coencapsulating doxorubicin (dox) and [Gd(HPDO3A)(H_2O)], and injected in tumor-bearing rats before MR-HIFU treatment. Four treatment groups were defined: hyperthermia, ablation, hyperthermia followed by ablation, or no HIFU. The intratumoral TSL and dox distribution were analyzed by single-photon emission computed tomography (SPECT)/computed tomography (CT), autoradiography, and fluorescence microscopy. Dox biodistribution was quantified and compared with that of nonliposomal dox. Finally, the treatment efficacy of all heating strategies plus additional control groups (saline, free dox, and Caelyx) was assessed by tumor growth measurements. All HIFU heating strategies combined with TSLs resulted in cellular uptake of dox deep into the interstitial space and a significant increase of tumor drug concentrations compared with a treatment with free dox. Ablation after TSL injection showed [Gd(HPDO3A)(H_2O)] and dox release along the tumor rim, mirroring the TSL distribution pattern. Hyperthermia either as standalone treatment or before ablation ensured homogeneous TSL, [Gd(HPDO3A)(H_2O)], and dox delivery across the tumor. The combination of hyperthermia-triggered drug delivery followed by ablation showed the best therapeutic outcome compared with all other treatment groups due to direct induction of thermal necrosis in the tumor core and efficient drug delivery to the tumor rim.

focused ultrasound | drug delivery | temperature-sensitive liposomes | ablation | hyperthermia

Heat is one of the oldest weapons in the armamentarium against cancer, with hyperthermia (40–45 °C) and cautery well documented in ancient medical literature (1–3). After centuries of clinical use, hyperthermia is finally starting to receive recognition as an efficient sensitizer of radiotherapy and chemotherapy with recent milestone clinical trials proving its efficacy (4–15). Cautery using a glowing iron has fortunately been replaced with minimally invasive techniques for local thermal ablation (55–60 °C) of neoplasms using, for example, light, microwave, radiofrequency (RF), or high-intensity focused ultrasound (HIFU) (16). Here, the cancerous lesion is heated to temperatures that induce cell death via coagulative necrosis in the central thermal treatment zone. The latter is surrounded by a peripheral zone, where temperatures shortly reach hyperthermic levels via heat diffusion that are sublethal, causing upmost transient effects on perfusion, cells, or the tumor microenvironment. The peripheral zone is therefore the most likely source for local recurrence from occult cancer cells that were spared in an attempt to limit the damage to vital tissue structures surrounding the tumor (17–19), which is a recognized issue in ablative therapies (20, 21). Therefore, adjuvant and adjunct therapies for treatment of the peripheral danger zone are highly warranted. Systemic administration of chemotherapeutic drugs is often used in the battle against occult cancer cells but is associated with severe side effects, which, besides being a major burden for the patient, limit the therapeutic window of the treatment. Hyperthermia-triggered drug delivery, first investigated decennia ago, may offer a solution to this problem (22, 23). In this approach, chemotherapeutic drugs are stably encapsulated in the aqueous lumen of temperature-sensitive liposomes (TSLs) at body temperature but are released at hyperthermic temperatures. Noninvasive heating of a malignant tissue will therefore trigger local drug release, leading to high local concentration of chemotherapy. However, drug delivery by TSLs is dependent on the presence of functional blood vessels, which is not self-evident in the tumor core, often being necrotic and poorly perfused. Therefore, the concept is being applied in a (neo) adjunctive fashion. For example, this concept has been taken into clinical trials as an adjunct therapy for the treatment of the peripheral zone during RF ablation of liver metastasis (24). Although the clinical trial recently failed to reach the clinical endpoint, a subgroup analysis revealed beneficial effects for those patients where long enough heating times (>45 min) were achieved to ensure sufficient drug delivery (25). The underlying problem is that current ablative technologies do not allow controlled heating of the peripheral zone to hyperthermic temperatures

Significance

MRI-guided high-intensity focused ultrasound (MR-HIFU) is noninvasive technology able to focally heat tumor tissue from hyperthermic up to ablative temperatures. Although ablative temperatures can be used to destroy cancerous tissue directly, adequate ablation of tumor margins is often impossible due to the vicinity of vital structures, leaving a potential source for local recurrence. Another therapeutic option in oncology is hyperthermia-triggered local drug delivery using MR-HIFU in combination with temperature-sensitive liposomes (TSLs). In this study, we compare different MR-HIFU treatment schemes comprising ablation and hyperthermia-triggered drug delivery with respect to drug distribution and therapeutic efficacy. We show that a combination protocol of hyperthermia-induced drug delivery followed by ablation resulted in a homogeneous drug distribution and the highest therapeutic effect.

Author contributions: N.H., E.K., M.d.S., S.L., and H.G. designed research; N.H., E.K., M.d.S., and E.H. performed research; E.H. contributed new reagents/analytic tools; N.H., E.K., M.d.S., and E.H. analyzed data; and N.H., E.K., M.d.S., S.L., and H.G. wrote the paper.

Conflict of interest statement: E.H. and S.L. are employed by Philips Research, The Netherlands.

This article is a PNAS Direct Submission.

[1]N.H. and E.K. contributed equally to this work.

[2]To whom correspondence should be addressed. Email: holger.gruell@uk-koeln.de.

This article contains supporting information online at www.pnas.org/lookup/suppl/doi:10.1073/pnas.1700790114/-/DCSupplemental.

www.pnas.org/cgi/doi/10.1073/pnas.1700790114

for a sufficiently long time span. Instead, hyperthermia in the peripheral tumor zone is achieved by heat diffusion during ablation of the central zone (26). HIFU is a noninvasive heating technique that allows both ablation of the central tumor zone, and prolonged hyperthermia of the tumor periphery, thereby addressing the above-mentioned shortcomings. HIFU uses focused sound waves for heating of s.c. to deep-seated tissues. When performed under magnetic resonance guidance (MR-HIFU), in vivo mapping of the induced temperature change is used as a feedback for accurate heating of the tissue over an extended time period (27, 28). Currently, MR-HIFU is the only technique that can perform ablation and well-defined hyperthermia in one session using user-defined protocols in terms of temperatures, time spans, thermal dose, and targeted volumes that may differ for ablation and hyperthermia. In a preclinical setting, MR-HIFU has been used either for ablation or for hyperthermia-triggered drug delivery (29–37), but so far no study exists that experimentally examined more complex thermal protocols, their combination with temperature-induced drug delivery, and their effect on cancer treatment.

In our study, we set out to investigate MR-HIFU thermal therapies with complementary intravascular doxorubicin (dox) delivery from TSLs in a preclinical setting using a rhabdomyosarcoma rat tumor model. First, the effect of different HIFU heating strategies [i.e., hyperthermia, ablation, and hyperthermia followed by ablation (hyp-ab)] on the drug delivery process was visualized via changes in longitudinal relaxation rate (R_1) as a result of the release of coencapsulated MR contrast agent [Gd(HPDO3A)(H_2O)] as shown previously by several groups (33, 38–41). The fate of the liposomal carrier was probed by radiolabeling of the carrier using a small fraction of 1,4,7,10-tetraazacyclododecane-1,4,7,10-tetraacetic acid (DOTA)–1,2-distearoyl-*sn*-glycero-3-phosphorylethanolamine (DSPE) lipid incorporated in the phospholipid membrane (41). The distribution of the drug was evaluated both by fluorescent microscopy (34, 42) and by quantification of the ^{14}C-doped dox using liquid scintillation counting. Finally, the therapeutic effect of the different HIFU heating strategies with and without adjuvant localized drug delivery was compared with that of clinically applied treatments with free dox and Caelyx in a tumor growth delay study. A schematic overview of the study groups is provided in Fig. 1.

Results

Liposomes. The TSLs had a hydrodynamic radius of 60.8 ± 0.7 nm (polydispersity index, 0.07 ± 0.02). The average molar ratio of dox over phosphate was 0.069 ± 0.009, whereas the Gd over phosphate ratio was 0.50 ± 0.04. The TSLs were stable at 37 °C while showing fast and quantitative release at 42 °C (Fig. S1). The incorporation of 1 mol% DOTA-DSPE in the phospholipid bilayer did not affect the stability of the liposomes at 37 °C, nor the dox release at 42 °C as was shown previously (41).

Contrast Agent Release. The R_1 maps obtained at various stages during the different HIFU treatments are depicted in Fig. 2. The average R_1 over time for the different HIFU treatment regimens is shown in the appendix (Fig. S2), and the statistical tests performed are listed in Table S1. TSL injection followed by hyperthermia resulted in an increase in tumor R_1 after the first 15-min hyperthermia session (15 min vs. pretreatment: $\Delta R_1 = 0.12 \pm 0.09$ s^{-1}, $P = 1 \times 10^{-4}$), whereas the second hyperthermia session did not induce a further R_1 increase (30 min vs. pretreatment: $\Delta R_1 = 0.12 \pm 0.08$ s^{-1}, $P = 0.679$). The R_1 had partly decreased again by the end of the scan session (90 min vs. pretreatment: $\Delta R_1 = 0.11 \pm 0.06$ s^{-1}, $P = 0.031$). No significant increase of R_1 was observed in the adjacent muscle (15 min vs. pretreatment: $\Delta R_{1,muscle} = 0.013 \pm 0.058$ s^{-1}, $P = 0.397$). TSL injection without HIFU resulted in much smaller R_1 changes in tumor (30 min vs. pretreatment: $\Delta R_1 = 0.071 \pm 0.071$ s^{-1}, $P = 0.040$), which were comparable to those in surrounding muscle (30 min vs. pretreatment: $\Delta R_{1,muscle} = 0.034 \pm 0.13$ s^{-1}, $P = 0.259$). This suggested that the liposomal content was not actively released from the TSLs in the unheated tumors.

In the tumors that were treated with ablation plus TSL, an increase in R_1 was typically observed along the rim of the tumor, whereas several tumors showed an increase in the tumor core as well as in the surrounding muscle tissue after ablation (Fig. 2). The average R_1 across the entire tumor showed a significant increase compared with the preinjection value ($\Delta R_1 = 0.44 \pm 0.31$ s^{-1}, $P < 0.001$). R_1 did not show a significant decrease 90 min after TSL injection as opposed to immediately after the ablation plus TSL (90 min vs. pretreatment: $\Delta R_1 = 0.50 \pm 0.25$ s^{-1}, $P = 0.163$), suggesting trapping or reduced clearance of the released contrast agent because of local damage to the vasculature. Contrast agent release was also observed in the muscle tissue surrounding the ablated tumor (after ablation vs. pretreatment: $\Delta R_1 = 0.14 \pm 0.16$ s^{-1}, $P = 0.001$). In the hyp-ab treatment group, the first hyperthermia

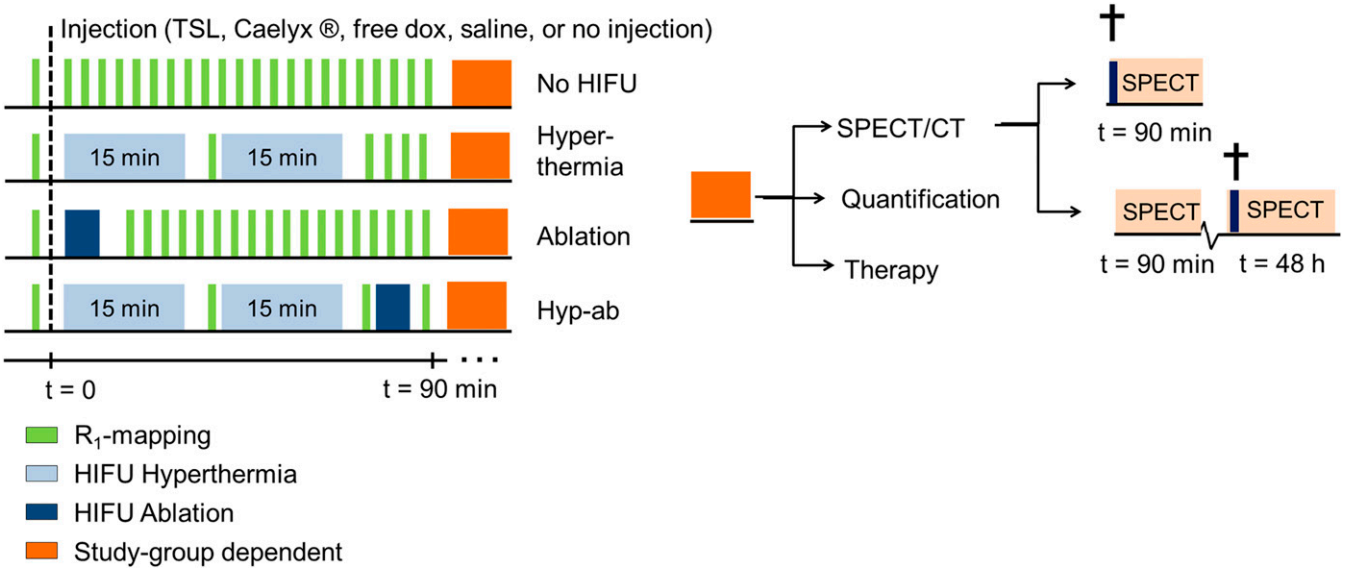

Fig. 1. Schematic overview of the timelines for each of the applied MR-HIFU thermal therapy strategies in the different substudies used to investigate the drug delivery patterns and therapeutic efficacy.

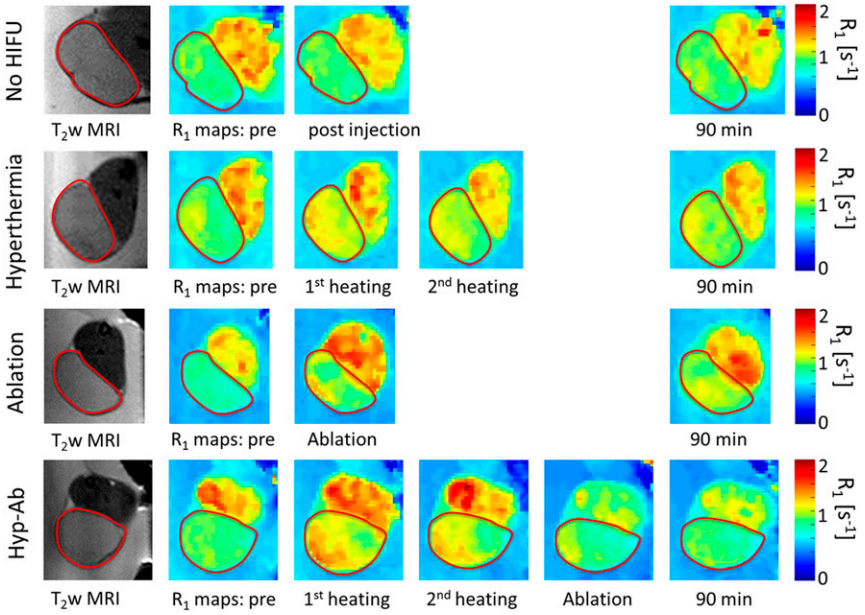

Fig. 2. Maps of the longitudinal relaxation rate (R_1) preinjection and after each heating step. The red contour indicates the tumor location.

treatment initially induced a homogeneous R_1 change (15 min vs. pretreatment, $\Delta R_1 = 0.12 \pm 0.07\ s^{-1}$, $P = 2 \times 10^{-5}$), which was maintained during the second hyperthermia treatment (30 min vs. pretreatment, $\Delta R_1 = 0.13 \pm 0.07\ s^{-1}$, $P = 0.852$), as was also seen in the hyperthermia-plus-TSL group. The ablation step following hyperthermia treatment led to a very variable R_1 change (ablation vs. pretreatment: $\Delta R_1 = 0.14 \pm 0.19\ s^{-1}$, $P = 0.003$) and a reduced washout (90 min vs. pretreatment: $\Delta R_1 = 0.38 \pm 0.27\ s^{-1}$, $P = 0.917$).

Distribution of ^{111}In-Labeled Liposomes. The uptake and tumor distribution of the TSLs was analyzed by means of single-photon emission computed tomography (SPECT) imaging, gamma counting, and autoradiography. The statistical tests performed are listed in Table S1; P values that are mentioned are acquired by post hoc testing. Ninety minutes after TSL injection, the amount of liposomes in the tumor was similar for most heating strategies, except for the hyp-ab treatment, which led to higher liposome concentration than observed in the group receiving no HIFU (Fig. 3*A*, $P = 0.029$). All treatment groups showed a trend of increasing TSL concentration over time (Fig. 3, values of $P < 0.1$). This trend could also be observed in the two SPECT scans performed on the animals that were euthanized 48 h after TSL injection (once in vivo 90 min postinjection, and once after euthanization), except for the animals that received no HIFU treatment (Fig. S3).

In terms of tumor distribution, a clear distinction was observed between the animals treated with hyperthermia plus TSL and with ablation plus TSL (Fig. 4). Hyperthermia-plus-TSL treatment resulted in a homogeneous uptake of the liposomes over the tumor area. In the animals that were treated with ablation immediately after TSL injection, the majority of the activity was located on the rim of the tumor. For the hyp-ab–plus–TSL group, a homogeneous baseline uptake was visible in the entire tumor, with occasional enhanced areas (Fig. 4). There was no change in the distribution patterns over the tumors between the 90-min and the 48-h group. These findings were confirmed by autoradiography on the middle slice of each tumor (Fig. 5 and Fig. S4). Photographs of the tumor slices revealed dark red areas after ablation-plus-TSL treatment,

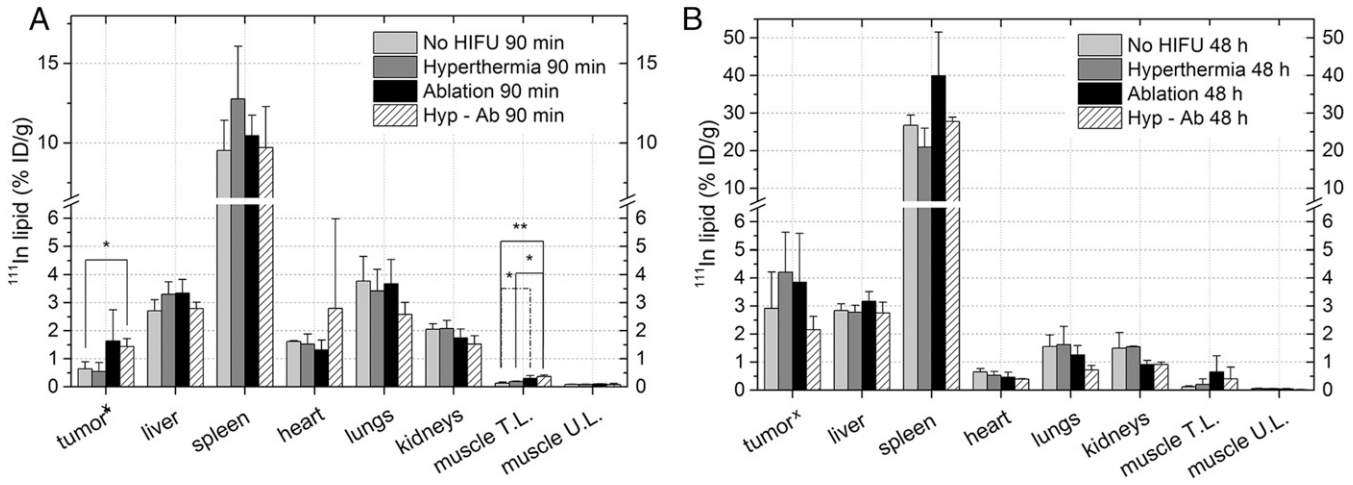

Fig. 3. Biodistribution of ^{111}In-lipid 90 min (*A*) or 48 h (*B*) after TSL injection as measured by dose calibrator (*tumor) or by gamma counting (all other organs). The average change and the SD per group are shown. The asterisk (*) indicates a significant difference (*$P < 0.05$, **$P < 0.01$). Muscle T.L. and U.L. are the muscle on the treated leg and the untreated leg on the contralateral side.

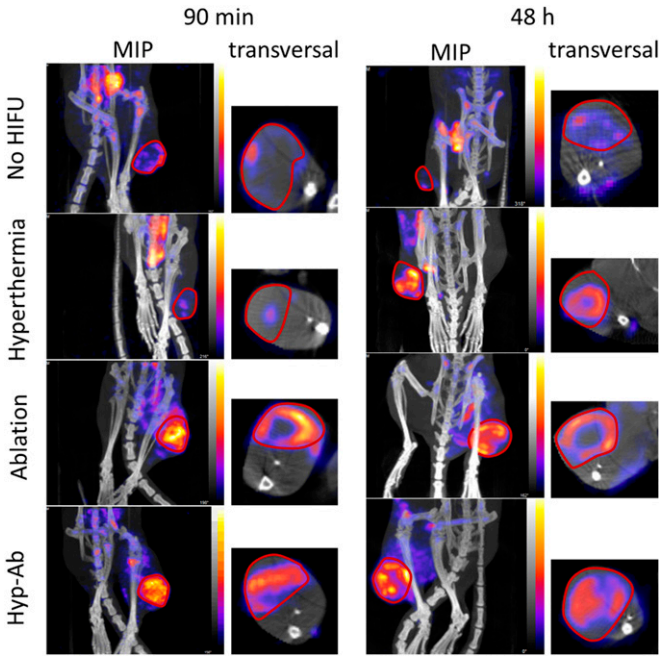

Fig. 4. Representative SPECT/CT images 90 min and 48 h after ^{111}In-labeled TSL injection for each of the HIFU heating strategies and the no-HIFU group. Both an overview maximum intensity projection (MIP) of the lower extremities is shown, as well as a transversal slice through the center of the tumor.

indicating areas of local hemorrhage, which were not observed in animals that received no HIFU previously (34). These areas colocalized with the areas of high activity visible on autoradiography, suggesting TSL accumulation in the extravascular area due to local vascular damage (i.e., hemorrhage). Considering the equivalent liposome uptake in all heat-treated tumors, this implied that the liposome concentration in the border zones of the ablated tumors was higher than the average liposome concentration observed in the hyperthermia-treated tumors.

Apart from analyzing the tumor uptake, the biodistribution of the ^{111}In-labeled TSLs in the rest of the animal was analyzed postmortem using gamma counting (Fig. 3*A* and Fig. S5). In the animals in which the treatment protocol comprised an ablation step, a significant increase in activity was observed in the muscle surrounding the ablated tumor 90 min after injection (hyp-ab plus TSL > no HIFU plus TSL and hyperthermia plus TSL, ablation plus TSL > no HIFU plus TSL). No effect of the different HIFU heating strategies was found on the TSL uptake in the contralateral leg muscle and in the leg bones, or in the other tissues examined (Fig. 3 *A* and *B* and Fig. S5). At 48 h, the activity was mainly present in the spleen and liver, consistent with uptake of the liposomes by the reticuloendothelial system (Fig. 3*B*).

Histology. While the above analysis studied the distribution of the TSL drug carrier for different treatment strategies, the effect on the local distribution of the drug in the tumors was analyzed using fluorescence microscopy. The current histology data complement the data published earlier, showing the dox distribution 90 min and 48 h after TSL injection for no HIFU and for hyperthermia (34). Larger areas were reached by the drug, and cellular uptake of the drug was visible even at relatively long distances from the blood vessels after hyperthermia-plus-TSL treatment (~50 μm, 90-min group). After 48 h, uptake of dox by the tumor cell nuclei was also observed in the animals that did not receive HIFU treatment.

Ablation-plus-TSL treatment resulted in areas with nonviable cells by nicotinamide adenine dinucleotide (NADH) staining 90 min after TSL injection (Fig. 6*A*). On the fluorescence images, the nonviable areas showed markedly lower dox uptake than the viable parts of the same tumor. Some areas that were still viable on NADH staining had a low fluorescence intensity, indicating a low concentration of doxorubicin. A band with high fluorescence intensity was evident along the tumor rim surrounding the area with low fluorescence intensity. When these areas were magnified, similar uptake of dox by the tumor cell nuclei was observed as after hyperthermia-plus-TSL treatment, including the uptake at relatively large distance (~50 μm) from the blood vessels (Fig. 6*A*, magnification). Forty-eight hours after ablation, some areas with high dox fluorescence intensity remained viable on the NADH staining (Fig. 6*B*).

Uptake of dox by the tumor cell nuclei was also evident in the animals that were treated with both hyperthermia and ablation after TSL injection (hyp-ab plus TSLs, Fig. 6*C*). There was no band of high fluorescence intensity visible around the ablated area, suggesting that the ablation step following the hyperthermia treatment did not add as much to the dox delivery as ablation directly after TSL injection. After 48 h, the nonviable areas colocalized with the areas of high fluorescence intensity, as was also observed after hyperthermia treatment alone (Fig. 6*D*) (34).

Doxorubicin Biodistribution. Ex vivo dox quantification was used to elucidate the efficiency of different treatment strategies in delivering dox to the tumor, evaluated at 90 min after injection (Fig. 7*A* and Fig. S5). The statistical tests performed are listed in Table S1. Significantly more dox was delivered in the tumors that were either treated with TSL injection followed by any of the heat treatments compared with the free dox (ablation plus TSL, hyperthermia plus TSL, hyp-ab plus TSL, all post hoc $P = 0.016$) or to no HIFU plus TSL (ablation plus TSL, hyperthermia plus TSL, hyp-ab plus TSL, all post hoc $P = 0.016$). No significant differences in tumor average dox concentration were observed between ablation plus TSL, hyperthermia plus TSL, or hyp-ab plus TSL. Although the dox concentration measured in the heart was comparable among all of the groups, due to the increased dox uptake in the tumor, an increased tumor-to-heart ratio was observed for all heat-treated groups compared with the free dox group ($P \leq 0.05$). The muscle adjacent to the tumor was only significantly affected in the ablation-plus-TSL group, which showed higher dox accumulation than the group injected with free dox or TSL

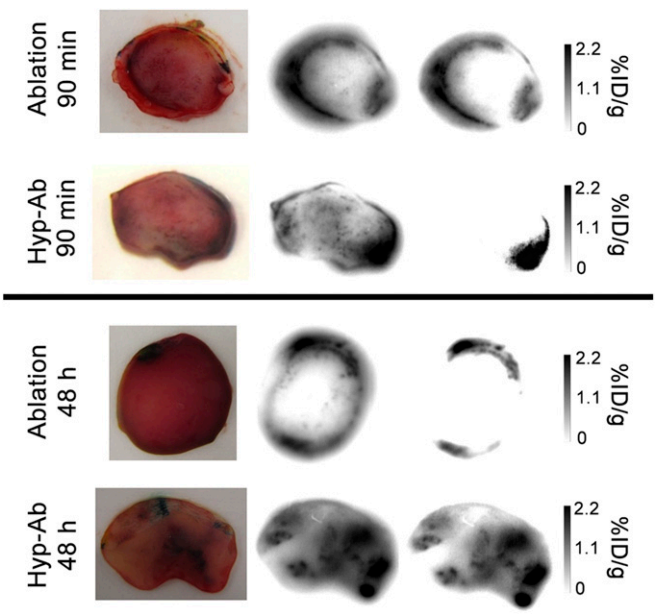

Fig. 5. Representative ^{111}In autoradiography slices through the center of the tumor after ablation and hyp-ab, both 90 min and 48 h after TSL injection. From *Left* to *Right*: tumor slice picture, unscaled autoradiographic image, and autoradiographic image scaled to the total percentage of the injected dose per gram tissue activity uptake in the slice.

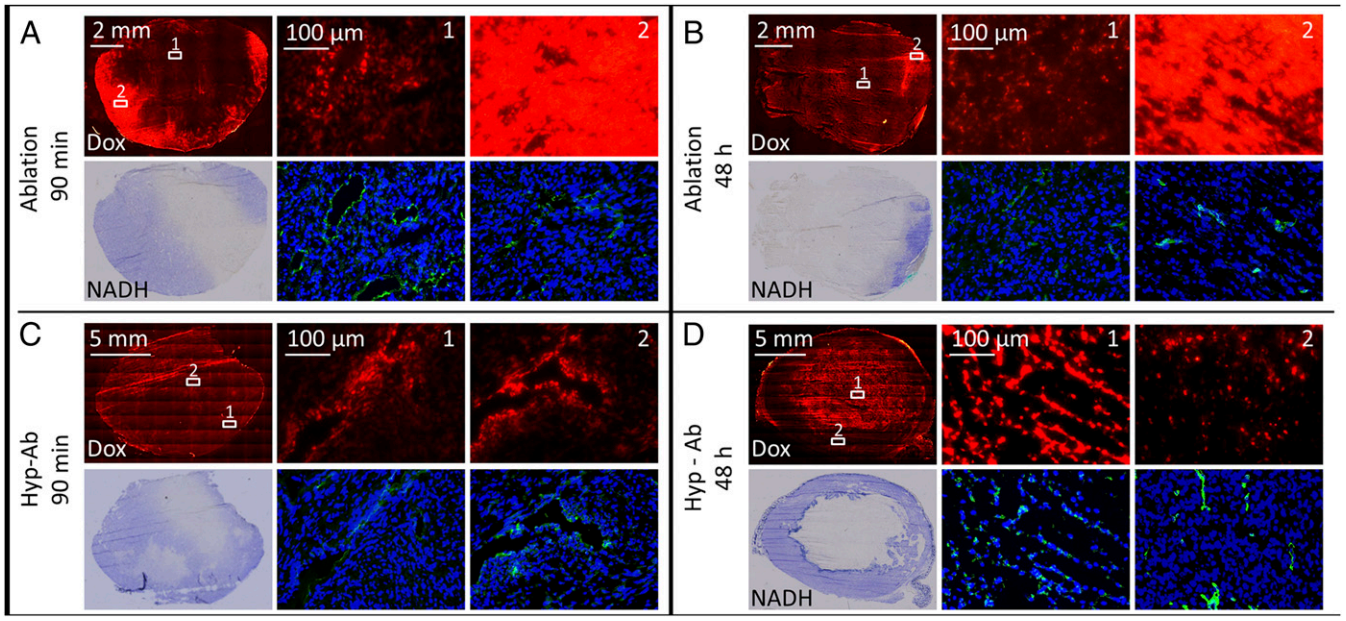

Fig. 6. Histological assessment of tumors treated with HIFU ablation (*A* and *B*) and hyperthermia followed by ablation (hyp-ab) (*C* and *D*) 90 min and 48 h after TSL injection. The top row of each group shows the dox autofluorescence overview image (red, 3-s shutter time), followed by two magnified dox images (red, all acquired at 1-s shutter time to allow for comparison). The bottom row of each group shows an NADH-diaphorase overview image (blue, viable cells; white, nonviable cells), followed by CD31 (green) and DAPI (blue)-stained magnified images acquired at the same location as the dox magnified images.

without heating (no HIFU plus TSL) ($P = 5.0 \times 10^{-4}$ and $P = 0.042$, respectively).

Although free dox was almost completely cleared from the blood 90 min after injection [0.16 ± 0.06% injected dose (ID)/g], there was still a substantial amount of dox present in the blood samples of the animals in the no-HIFU group (9.9 ± 1.6%ID/g), which was significantly higher than the amount of dox in the blood for all other treatment groups except for the hyp-ab–plus–TSL group ($P < 0.02$). Dox was cleared by the liver, spleen, and kidney. The liver of the animals subjected to free dox injection has a higher dox concentration than that of the animals injected with TSL, regardless of the heat treatment administered ($P < 0.01$).

The percentage of injected dose of dox in the tumor (Fig. 7*A*) was compared with that of the animal groups injected with ^{111}In-labeled liposomes (Fig. 3*A*). No significant difference between dox and ^{111}In-labeled liposomes was detected for the no-HIFU–plus–TSL group ($P = 0.19$) and the group that was subjected to ablation plus TSL ($P = 0.19$). On the other hand, the tumors of the animals treated by either hyperthermia-plus-TSL or the hyp-ab–plus–TSL treatment contained a significantly higher amount of dox than ^{111}In-labeled liposomes, suggesting intravascular release and subsequent uptake of dox after prolonged hyperthermia treatment ($P = 0.036$ and 0.016, respectively).

The dox concentration in the tumor vs. the R_1 change right after the last heat treatment (or 30 min after injection for the no-HIFU group) is plotted in Fig. 7*B*. For all groups, $n = 4$ or 5 (Table 1), except for the no-HIFU group due to image artifacts in the R_1 map in two animals ($n = 3$). Treatments comprising an

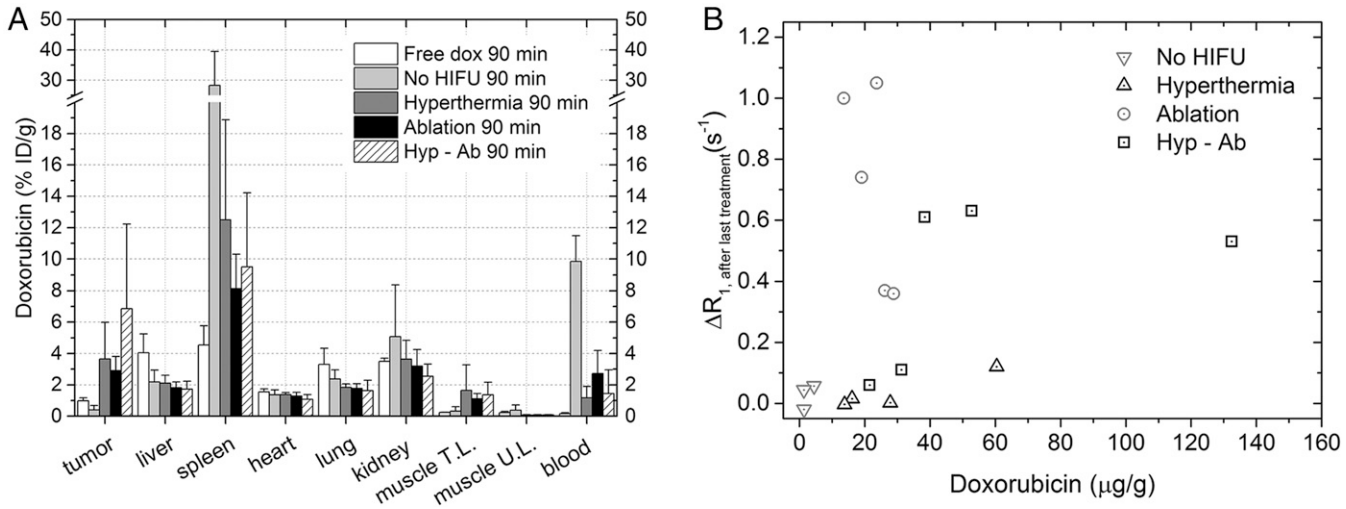

Fig. 7. (*A*) Biodistribution of dox 90 min after injection of the TSLs as measured by liquid scintillation counting. The average change and the SD per group are shown. (*B*) Tumor dox concentration 90 min after injection of the TSLs after various heat treatments, plotted against the R_1 change observed right after the last heat treatment (or in case of the no HIFU group, 30 min after injection of the TSLs).

Table 1. Overview of the number of animals in every group

Study group	Injection	HIFU treatment: No HIFU	Hyperthermia	Ablation	Hyp-Ab
SPECT and histology (90 min + 48 h)	TSL	4 + 3*	3 + 3*	4 + 3	4 + 3
Dox quantification	TSL	5	5	5	5
	Free dox	5	—	—	—
Therapy	TSL	6	6	5	7
	Free dox	5	6	—	—
	Caelyx	5	5	—	—
	Saline	5	5	—	—
	No injection	—	—	6	—

*The histology and autoradiography data from this group were previously published in de Smet et al. (34).

ablation generally showed higher R_1 changes than the hyperthermia plus TSL or tumors that received no HIFU. When all groups were evaluated together, no meaningful correlation existed between the R_1 values and the average tumor dox concentration ($R^2 = 0.05$). When the no-HIFU–plus–TSL and hyperthermia-plus-TSL groups were evaluated together, a weak correlation ($R^2 = 0.43$, $n = 7$) was detected.

Therapeutic Efficacy. In a separate group of animals, the therapeutic efficacy of the different heating strategies in combination with TSL on the tumor growth control was studied and compared with that of several control groups. The relative tumor growth over time for the individual animals of the 11 treatment groups is shown in *Supporting Information* [TSL injection followed by hyperthermia and ablation (group 1), TSL injection followed by ablation (group 2), TSLs, Caelyx, free dox, or saline injection with or without hyperthermia (groups 3–10), ablation only (group 11)] (Fig. S6*A*). There was no statistically significant difference in the pretreatment tumor volumes between the different groups (727 ± 242 mm^3; ANOVA, $P = 0.707$). Some animals showed an initial increase in tumor size directly after ablation or combination treatment, most likely due to treatment-induced edema, which could not be distinguished from the actual tumor volume with the caliper measurements used. After the initial increase, all treated tumors showed a delay in growth compared with tumors that were not treated. The average minimum body weight of the different groups, a measure of toxicity, showed no significant differences (one-way ANOVA, $P = 0.17$; Fig. S7).

In Fig. 8, the tumor size-related time of survival is plotted for the different treatment groups. The efficacy of the treatment was judged based on the time point the tumor reached three times the pretreatment tumor volume. This time point was derived from the fitted tumor growth curves. A log-rank analysis indicated that the control groups TSL, Caelyx, free dox, saline injection and Caelyx, free dox, saline injection plus hyperthermia all behaved similarly. Adding any type of heat treatment to a TSL injection led to a decrease in tumor growth, as was the case for the ablation group (without TSL injection). Finally, TSL injection with hyperthermia followed by ablation treatment (hyp-ab + TSL) showed the largest effect on the tumor growth in time, outperforming all of the other treatments. The log-rank results are presented in *Supporting Information* (Table S2).

Discussion

In this study, the effects of HIFU heating strategies on the biodistribution of TSL and dox, the intratumoral dox distribution, and their respective therapeutic efficacies were investigated. Our hypothesis was that hyperthermia treatment would lead to a large amount of dox delivered to vascularized tumor areas with improved intratumoral distribution, whereas ablation is beneficial for direct destruction of the more necrotic tumor core with temperature-induced drug delivery along the border zone surrounding the ablated volume. For the latter, drug delivery may be compromised by temporal vascular shutdown in the intermediate zone surrounding the ablated volume, and by the rather short time span at hyperthermic temperatures reached during the ablation (43). Therefore, we added a hyp-ab–plus–TSL group in which the ablation step was preceded by 30 min of hyperthermia to ensure upfront dox accumulation in well-perfused areas. For the hyp-ab heating strategy, we expected efficient drug delivery to well-perfused tumor parts combined with direct heat-inflicted cytotoxicity to poorly perfused or necrotic areas leading to an overall synergistic effect in tumor growth delay.

For all groups, an increasing liposomal uptake in tumors was observed over time due to the "enhanced permeability and retention (EPR) effect" intrinsic to most tumor tissues (44, 45). It is previously reported that hyperthermia can increase the EPR-driven uptake of liposomes in the tumor (41, 46–48), which could lead to additional dox uptake from residual nonreleased TSLs over time. However, this increase in EPR effect can be tumor-dependent (46) and for the R1 rhabdomyosarcomas studied here, no HIFU-induced increase in EPR effect was observed as all groups showed comparable TSL uptake 48 h after injection. For both hyperthermia-treated animals and animals that did not receive HIFU treatment, SPECT imaging showed a relatively homogeneous uptake across the tumor, with a trend of increasing TSL concentration over 48 h. Although uptake of TSLs is a slow process with typical maximum tumor concentration reached after 8–48 h (46), the therapeutically relevant process is the intravascular release of dox from TSLs, which takes place while hyperthermia is applied, that is, within the first 40 min after injection of TSLs. Numerous preclinical studies using comparable TSL formulations have shown that hyperthermia-induced intravascular release of dox from TSLs typically led to higher tumor concentrations compared with control groups at normothermia, although strong intertumoral variations were observed depending on the tumor morphology (29, 32, 33, 36, 49). Similarly, in this study, the

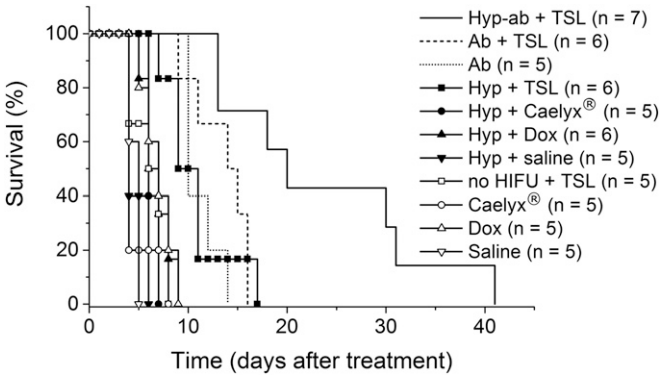

Fig. 8. Survival analysis based on the time point the tumor reached three times the pretreatment tumor volume. Ab, ablation; Dox, free doxorubicin; Hyp, hyperthermia.

hyperthermia treatment led to a median tumor dox concentration of factor 14.6 higher tumor dox concentration compared with the no-HIFU group (median 2.840%ID/g vs. 0.194%ID/g) and a factor 2.9 times higher than the free doxorubicin group (median, 2.840%ID/g vs. 0.985%ID/g). Free dox and Caelyx, a non–temperature-sensitive liposomal dox formulation, are the clinical standard dox-based chemotherapeutic treatments for several malignancies (50, 51). Although no "non-TSL formulation" such as Doxil/Caelyx was included in the quantification study, the TSL–plus–no-HIFU group is expected to be comparable in drug delivery at normal temperature within the 90-min time point due to the high dox encapsulation stability of TSLs (41). Importantly, in previously published research, histology showed that the hyperthermia treatment improved the bioavailability of the dox as the drug reaches cells farther away from the tumor vessels than it would for the treatment without HIFU (34, 52, 53). While the free drug diffuses along a strong concentration gradient from the blood vessel into the tumor tissue, the diffusion of dox encapsulated in TSLs is limited by the size of the TSLs.

For ablation-plus-TSL group, both dox and TSLs predominantly accumulated in the tumor rim surrounding the ablated tumor area, where no accumulation of dox nor TSLs was observed. As the average tumor dox and TSL concentration were comparable to those in the hyperthermia-treated tumors, the local concentrations of both dox and TSLs in the rim must be higher. The accumulation pattern of TSLs and dox was congruent with areas of tumor hemorrhage visible on anatomical T_2*-weighted MR images and microscopy slides in tissues surrounding the ablated area. The comparable intratumoral distribution pattern of dox and TSLs is a result of trapping due to vascular shutdown (43) as well as local liposome extravasation and hemorrhage owing to vascular damage in tissue adjacent to the ablated zone (54). Interestingly, in between the outer rim containing a high dox concentration and the inner, heat-destroyed nonviable tumor tissue, an intermediate zone exists that does not contain dox yet is still viable. Here, the sublethal temperature dose during the short ablation time span caused a temporal vascular shutdown prohibiting perfusion and intravascular release of dox from TSLs that created an undertreated danger zone surrounding the ablated tumor volume (18, 55).

Hyp-ab–plus–TSL treatment showed a significant enhanced uptake of TSLs in the tumor compared with the no-HIFU–plus–TSL group 90 min after injection. Both the dox and the TSL distribution were comparable to the hyperthermia-plus-TSL group, with some additional hemorrhage at the tumor rim. The tumor-averaged dox concentration (in micrograms per gram; Fig. S5*C*) for this group is approximately two times higher than the hyperthermia-plus-TSL or ablation-plus-TSL group, although strong intertumoral variations led to a large SD and therefore no statistical significance. Remarkably, our findings correspond well with a simulation performed by Gasselhuber et al. (43) for HIFU-induced drug delivery for the hyperthermia and hyp-ab heating schemes. The ablation step in the hyp-ab protocol causes a vascular shutdown restricting perfusion, which in turn leads to increased dox uptake over time as backdiffusion of dox from the extravascular extracellular space to the plasma is strongly reduced. The simulations predict for the hyp-ab protocol a roughly 1.5 times higher intracellular dox concentration compared with the hyperthermia alone 90 min after injection (43). Furthermore, our absolute dox tissue concentration of the different groups (Fig. S5*C*) are consistent with the predicted concentrations by Gasselhuber et al. as well.

All heat treatments combined with TSLs led to a significant increase in R_1 immediately after, indicating the release of contrast agent from the TSLs. For the hyperthermia and no-HIFU groups, we find a correlation between the R_1 change after hyperthermia and tumor drug concentration ($R^2 = 0.43$ after the second hyperthermia treatment), similar to other literature studies (32, 33, 56). As the R1 rhabdomyosarcoma tumor model exhibits better structured blood vessels reflected by a lower K_{trans} and v_e compared with the earlier used 9L model (34), a lower concentration of the released MRI contrast agent in the tumor is likely in the R1 rhabdomyosarcoma model. This is reflected in an overall smaller increase of the longitudinal relaxation rate R_1 per percent injected dose per gram dox measured after the treatment is completed (Fig. S8) (33, 41). For the ablation-plus-TSL group, a noticeable R_1 increase was observed in the range of 0.12–1.05 s^{-1} caused both by release or trapping of the contrast agents (57) in the outer rim and an additional R_1 change intrinsic for ablated tissue. Ablation-induced R_1 increases were measured by others and were attributed to the increased access of tissue water to paramagnetic blood iron due to the heat-induced denaturation of hemoglobin and the disruption of biological barriers (58, 59). The R_1 change due to ablation also obscured the relation between ΔR_1 and the intratumoral dox concentration for the hyp-ab–plus–TSL group. Although this complicates the calculation of the amount of drug that was delivered, it can give information on the extent of the ablation (55).

The therapeutic effect of the different HIFU heating strategies combined with local drug delivery was evaluated in a tumor growth study and compared with several control treatments, among others the clinically relevant Caelyx and free dox, which are the clinical standard for chemotherapeutic treatment of a number of malignancies (50, 51). The dox dose was sufficient to significantly improve the survival in the group injected with free dox compared with the group that only received saline injection. The control groups injected with Caelyx and TSL without HIFU showed comparable survival as the group injected with free dox (60–62). The addition of a hyperthermia treatment neither improved the treatment effect of free dox nor of Caelyx. Although hyperthermia typically enhances extravasation of liposomes (47, 48, 63), dox encapsulated in the non–temperature-sensitive liposomal formulations of Caelyx does not become bioavailable. In contrast, hyperthermia in combination with TSL induces intravascular release of dox ensuring its bioavailability and improved tumor penetration, which is reflected in improved efficacy of hyperthermia plus TSLs over hyperthermia plus Caelyx. Interestingly, the hyperthermia-plus-TSL group performs comparably to the ablation-plus-TSL and also the regular ablation group. Quantitative ablation of the tumor including a safety margin around was impossible in our s.c. tumor located between skin and adjacent muscle layer, with risking either severe skin burns or impaired limb movement due to unintentional ablation of the femoral or saphenous nerves. This situation is similar to the clinical situation, where ablation of the entire tumor volume is often challenging, because crucial surrounding structures need to be spared. The combination of ablation and TSLs led to areas with temporarily vascular collapse, which did not result in coagulative necrosis (18). We believe these undertreated areas with viable tumor tissue are the source for recurrent tumor growth leading to similar therapeutic outcome as observed in the hyperthermia-plus-TSL and ablation groups. For the combination protocol, we observed the largest survival benefit, as the first hyperthermia drug delivery treatment ensured efficient dox delivery and tumor penetration in well-perfused areas, whereas the subsequent ablation of the tumor core would efficiently treat poorly perfused parts combining the advantages of both approaches.

Despite the initial delay in tumor growth that was observed in most treatment groups (Fig. S6), no complete tumor remission was achieved for any treatment scheme. Beside the aforementioned limitations to achieve quantitative tumor ablation, we chose a comparably low TSL dose of 2 mg dox/kg bodyweight in the therapeutic study (compared with the typically preclinically used dose of 5 mg dox/kg) (36, 40, 64) to avoid systemic side effects (65). Depending on the exact clinical application and also particular patient condition, a higher dose or repeated treatments schemes could be considered to further improve the therapeutic effect. For repeated treatments, the scheme should comprise multiple hyperthermia-mediated drug delivery sessions concluded by a final combination of hyperthermia and ablation to avoid intermediate vascular shutdown.

Localized drug delivery from TSLs in combination with MR-HIFU–induced hyperthermia and ablation was investigated here as an approach for obtaining improved local tumor control in a noninvasive manner. Depending on the tumor location and tumor

perfusion, prolonged HIFU-induced hyperthermia of large lesions is not suitable for every tumor and can be challenging in case of tumor motion. However, in recent years, the availability of HIFU (mostly for ablation purposes) has increased and technical hurdles for prolonged hyperthermia have been largely overcome (66, 67). Compared with regular chemotherapy, repeated application of HIFU plus TSLs would be more time-consuming and could potentially be interleaved with regular chemotherapy on a once a week treatment schedule comparable to clinically used hyperthermia treatment schedules (7). Regardless, we believe the combination of HIFU and TSLs is promising for certain tumors that do not respond well to chemotherapy alone (e.g., pancreatic cancer).

The need for additional chemotherapy as an adjunct to ablation treatment was previously rationalized for RF ablation treatment of larger (>3 cm^3) hepatocellular carcinoma (HCC) liver tumors (68). Tumor ablation using interstitial RF applicators in combination with dox-loaded TSLs (Thermodox) is currently undergoing randomized phase III clinical trials for treatment of HCC tumors (68–70). Early results showed the initial trial was not successful as the desired primary endpoint of showing 33% improvement in progression free survival had not been reached (24, 25, 71). However, post hoc analysis of the data showed that patient selection (single lesion only) and the duration of heating (>45 min), giving enough time for the liposomes to deposit high concentrations of dox, were key factors for successful clinical outcome leading to a greater than 2-y survival benefit (25). Because the delivered amount of drug directly relates to the heating duration, there is a clear rationale to resort to prolonged hyperthermia treatment ahead of the ablation treatment (43). Currently, MR-HIFU is the only device able to perform both prolonged hyperthermia and subsequent noninvasive ablation and would therefore be the ideal "one-stop shop" technology for drug delivery-supported ablation.

Conclusion

MR-HIFU is a powerful tool to induce localized tumor cell death by ablation. However, the presence of vital surrounding structures often hampers exhaustive treatment of the entire tumor volume plus a necessary safety margin. In this study, the combination of dox-loaded TSLs with various MR-HIFU heating strategies was investigated in a preclinical setting as a way to provide a more complete tumor treatment. We showed that both hyperthermia and ablation can be used as MR-HIFU heating strategy for enhancing TSL and dox accumulation in tumor tissue. Although comparable dox concentrations were reached regardless of the heating strategy, it did influence the distribution of the dox and TSL over the tumor. After ablation treatment, dox uptake was mainly observed in the tumor rim, whereas a zone surrounding the necrotic heat-fixated area remained that was still viable but did not contain any dox due to temporal vascular shutdown. The latter can be avoided using a hyperthermia-induced drug delivery treatment of 30 min before ablation, ensuring a more homogeneous dox delivery across the tumor. In a clinical setting, the hyperthermia-induced drug delivery step could be repeated several times using either MR-HIFU or other hyperthermia devices before concluding the treatment with a last combination of hyperthermia-triggered drug delivery followed by ablation. The exact clinical protocol for repeated studies needs future evaluation.

Materials and Methods

Materials. 1,2-Dipalmitoyl-*sn*-glycero-3-phosphocholine (DPPC) and hydrogenated-L-α-phosphatidylcholine (HSPC) were kindly provided by Lipoid (Germany). 1,2-Dipalmitoyl-*sn*-glycero-3-phosphoethanolamine-*N*-[methoxy(polyethyleneglycol)-2000] (DPPE-PEG2000) and cholesterol were purchased from Avanti Polar Lipids. DOTA-DSPE was synthesized using the procedure described by Hak et al. (72). Doxorubicin hydrochloride was purchased from AvaChem Scientific. [Gd(HPDO3A)(H_2O)] (ProHance) was obtained from Bracco Diagnostics (Italy). ^{14}C-doxorubicin hydrochloride, $^{111}InCl_3$, SOLVABLE, and Ultima Gold scintillation fluid were purchased from Perkin-Elmer.

TSLs. DOTA-functionalized TSLs composed of DPPC:HSPC:Chol:DPPE-PEG2000:DOTA-DSPE (50:25:15:3:1 molar ratio) were prepared for the SPECT/CT and histology study. For the tumor growth delay study and the dox quantification study, TSLs composed of DPPC:HSPC:Chol:DPPE-PEG2000 (50:25:15:3 molar ratio) were prepared (omitting DOTA-DSPE). The preparation, characterization, and optional indium-111 labeling of the TSLs was performed as described in de Smet et al. (41). For the dox quantification study, the liposome batch was split in two samples of which one was loaded with a dox solution doped with 46 ± 5 kBq/mg ^{14}C dox, whereas the other was loaded with cold dox solution to function as a cold analog for further characterization. The dox concentration was determined by liquid scintillation counting.

Animal Model. Syngeneic R1 rhabdomyosarcoma tumors were established in the hindleg of female Wag/Rij rats (Charles River; age, 5–7 wk) by s.c. implantation under anesthesia of pieces of donor tumor tissue (~1 mm^3) (73). Tumor sizes were determined by measuring the length (l), width (w), and depth (d) using a caliper, and the tumor volume was calculated by $0.5 \times l \times w \times d$. Animal studies were performed when the tumor reached a volume of >400 mm^3 (overall study, 738 ± 281 mm^3; therapy study, 727 ± 242 mm^3), typically 14–30 d after tumor implantation. All preclinical studies were approved by the animal welfare committee of Maastricht University (The Netherlands). The maintenance and care of the experimental animals were in compliance with the guidelines set by the institutional animal care committee, accredited by the National Department of Health and the guidelines set by the Guide for the Care and Use of Laboratory Animals (74).

MR-HIFU Treatment. The animals of the different study groups were subjected to one of four different HIFU treatments (Fig. 1 and Table 1). Preceding the HIFU treatment, they received an i.v. injection with either TSLs, Caelyx, free dox, saline, or no injection, depending on the study group. The first possible HIFU treatment was a sham treatment (no-HIFU group) during which the animal was brought under anesthesia but received no HIFU treatment. The second treatment consisted of two times 15 min of hyperthermia (hyperthermia group; average temperature, ~41 °C; continuous-wave ultrasound; acoustic frequency, 1.44 MHz; acoustic power, 10–15 W). The third treatment was an ablation treatment [thermal dose, >240 cumulative equivalent minutes at 43 °C ($CEM_{43\,°C}$); continuous-wave ultrasound; acoustic frequency, 1.44 MHz; acoustic power, 35 W]. The fourth treatment consisted of two times 15 min of hyperthermia, followed by ablation of the tumor core (hyp-ab group) (Fig. 1).

All animals received the same preparation before treatment, including shaving of the tumor-bearing leg and administration of a precautionary pain suppressor (carprofen; Rimadyl; 4 mg/kg body weight). They were positioned in the small animal MR-HIFU setup as developed by Hijnen et al. (27) using a clinical MR-HIFU platform (Philips Sonalleve). Respiration rate and body temperature of the animal were monitored continuously. The treatment was planned on T_2-weighted MR images acquired with a turbo spin echo scan [TSE factor, 7; repetition time (TR)/echo time (TE), 7,644/50 ms; field of view (FOV), 40 × 60 × 50 mm^3; voxel size, 0.5 × 0.5 × 0.6 mm^3; slices, 20; saturation bands, 2; acquisition time, 1:39 min]. Subsequently, a high-resolution fast-field echo scan was acquired to obtain more anatomical detail on the tumor (TR/TE, 800/13 ms; FOV, 40 × 48 × 20 mm^3; voxel size, 0.25 × 0.25 × 1.00 mm^3; slices, 20; flip angle, 20°; saturation bands, 1; number of averages, 2; acquisition time, 5:08 min). A map of the tumor longitudinal relaxation rate (R_1) was acquired using a single-slice Look Locker sequence [echo-planar imaging (EPI) factor, 5; TR/TE, 9.0/3.4 ms; FOV, 50 × 69 mm; matrix, 64 × 65; slice thickness, 2–5 mm; flip angle, 10°; fat suppression, spectral presaturation with inversion recovery (SPIR); half scan, 80%; interval time, 100 ms; time of inversion repetition, 6 s; number of averages, 2; acquisition time, 2:36 min], from which the apparent R_1* was obtained from the signal recovery on a voxel-by-voxel basis using an in-house created IDL-based software tool (IDL, version 6.3; RSI). The longitudinal relaxation rate (R_1) was derived from the apparent R_1* [R_1* = 1/T_1*, R_1 = R_1* + ln(cos(α))/TR, with α = 10° and TR = 100 ms] (75).

An ellipsoidal-shaped HIFU treatment cell (diameter, ~4 mm; length, ~10 mm) was positioned in the center of the tumor. For the hyp-ab treatment group, the ablation treatment cell was positioned at the same location as the hyperthermia treatment cell. Several low-power test sonications (continuous-wave ultrasound; acoustic frequency, 1.44 MHz; acoustic power, 5–10 W; duration, 20 s; typical temperature elevation, ~1–2 °C) were performed before therapeutic sonication to correct for possible focus point aberration. During sonication, proton resonance frequency shift-based MR thermometry was used to monitor the temperature changes in the target region. For hyperthermia monitoring, the temperature changes were continuously measured in two slices, one slice perpendicular and one slice parallel to the HIFU beam axis, both centered on the target area (RF-spoiled gradient echo with EPI readout; EPI factor, 7; TR/TE, 52/19.5 ms; FOV, 250 × 250 mm; matrix, 176 × 169; slice thickness, 4 mm; SENSE factor, 1.8; flip angle, 19.5°; fat suppression, SPIR; number of averages, 2; dynamic scan time, 2.4 s). During ablation treatment, the induced temperature changes were monitored using four slices, three subsequent slices perpendicular

to the beam axis and one slice parallel to the HIFU beam axis (dynamic scan time, 4.8 s). A zeroth-order phase correction was performed for baseline drift correction by subtracting the average phase in a reference region from the MR-acquired phase image, before the calculation of the temperature image.

Once the HIFU treatment had been planned and coregistered, the rats received an injection of TSLs, Caelyx, or free dox via a tail vein catheter at a dose of 5 mg dox/kg body weight (2 mg dox/kg body weight or a comparable saline volume for the therapy study). For animals injected with paramagnetic TSLs, R_1 maps were acquired in-between each heating period and after the last heating, followed by a T_2*-weighted fast field echo anatomical scan (Fig. 1). Rats were either allowed to recover and tumor growth was monitored over time (therapy group) or euthanized 90 min (SPECT group, dox quantification group) or 48 h (SPECT group) after TSL injection after which the tumor was dissected.

SPECT/CT Imaging, Autoradiography, and Gamma Counting. Three-dimensional information about the ^{111}In-lipid and therefore liposomal distribution in the tumors was obtained by imaging of the lower extremities using SPECT. The animals were euthanized 90 min or 48 h after ^{111}In-labeled Dox/Gd-TSLs (53 ± 16 MBq/mL liposome solution, 23 ± 5 MBq ^{111}In, 0.50 ± 0.2 mL) injection and were imaged by SPECT/CT. The animal numbers per group are listed in Table 1. For the animals that were euthanized after 48 h, an additional in vivo SPECT/CT scan was acquired 90 min after injection (Fig. 1). The measurements were performed on a small-animal SPECT/CT system (nanoSPECT/CT; Bioscan) equipped with four detector heads and converging nine-pinhole collimators (pinhole diameter, 2.5 mm; maximum resolution, 2 mm). The SPECT measurements (after euthanization: 24 projections, 200 s/projection, acquisition time of 60 min; in vivo: 24 projections, 100 s/projection, acquisition time of 30 min) were followed by an X-ray CT scan for anatomical reference (180 projections; tube voltage, 65 keV; exposure time, 1,500 ms; acquisition time, 9 min).

After scanning, the tumor slice corresponding to the middle of the HIFU treatment cell was marked using tissue dye. The entire tumor was dissected, and the ^{111}In activity in the tumor was measured using a dose calibrator (VDC-405; Veenstra Instruments). Subsequently, a tumor slice of 2-mm thickness was cut from marked area of the tumor using a stainless-steel tissue matrix (Ted Pella) for analysis of the ^{111}In-lipid distribution using autoradiography. The slices were weighed and exposed to a photostimulatable phosphor plate for a time varying from 4 h to 2 d, depending on the amount of radioactivity in the tumor slice. The exposed plates were scanned using a phosphor imager (FLA-7000; Fujifilm). The remainder of the animals was dissected and the radioactivity in blood, heart, lung, liver, spleen, left kidney, adrenals, intestines, skin, gastrocnemius muscle, and bones (femur, tibia, fibula) from both the treated and untreated leg was measured using a gamma counter (Wizard 1480; Perkin-Elmer). Known volumes of the injected TSLs were counted to serve as reference. The decay corrected radioactivity in the tissues was expressed as a percentage of the injected dose per gram tissue (%ID/g). The autoradiography data are only reported for the hyp-ab and ablation groups because the data for the hyperthermia and no-HIFU groups have previously been published (34).

Histology. For the animals that were subjected to SPECT/CT scans, the tumor parts that were not used for autoradiography were snap frozen in 2-methyl butane and stored at −20 °C before histological analysis. The frozen tissue was cut into 6-μm-thick slices ($n \geq 2$ per group). Fluorescence images of the dox distribution were acquired with a fluorescence microscope (Leica; DM6000B; DFC310FX camera) equipped with a custom-made dox filter set (excitation, 480/40 nm; emission, 600/60 nm; dichroic, 505 lp). Subsequently, the tissue slices were stained with CD31 to mark endothelial cells, DAPI to mark cell nuclei, NADH diaphorase to check for cell viability, and H&E to analyze the general morphology of the tissue. The histology data are only reported for the hyp-ab and ablation groups because the data for the hyperthermia and no-HIFU groups have previously been published (34).

Dox Quantification. In a separate group of animals (Table 1), dox concentrations were quantified in various tissues. The animals were randomly divided into five different treatment groups, being TSL injection followed by one of the aforementioned HIFU protocols (Fig. 1) and free dox injection ($n = 5$ per group). Animals in all treatment groups received 5 mg/kg dox spiked with ^{14}C dox before injection or before liposome loading (46 ± 5 kBq/mg). MR-HIFU treatment was performed as described above. The animals were euthanized by cervical dislocation 90 min after injection. Subsequently, pieces of various tissues were dissected (100–200 mg per tissue, except for the tumors, which were analyzed completely), and a blood sample was taken. The samples were homogenized at 4 °C with a stainless-steel ball for 30–60 min at 30 Hz using a Tissuelyzer (Qiagen). Homogenized blood and tissue samples were dissolved in solubilizer (Solvable) at 60 °C overnight. Decolorization was achieved by overnight incubation at 60 °C after the addition of 30% hydrogen peroxide and isopropanol [1:1 (vol/vol)]. Scintillation mixture (Ultima Gold) was added and the samples were counted with a liquid scintillation counter (Packard 2500 TR; 30 min/sample; energy window, 4–156 keV). Known volumes of the injected TSLs or free dox were counted to serve as reference.

Therapeutic Efficacy. The therapeutic effect of the different HIFU heating strategies in combination with drug delivery from TSLs was tested in a separate group of animals (Table 1) and compared with a group receiving only ablation and to various control groups (free dox, Caelyx, or saline, all with or without HIFU-induced hyperthermia). Animals in the groups without HIFU were kept under anesthesia for 1 h after the injection. The animals were allowed to recover after treatment, after which the tumor volume was monitored over time using a caliper (tumor volume $= 0.5 \times l \times w \times d$). The MR-HIFU treatment was performed as described above. The TSL dose was kept constant at 2 mg dox per kg body weight for all therapeutic groups. This dose was chosen to reduce side effects owing to the systemic toxicity of dox. From the tumor volume data, the relative tumor volume was calculated by dividing the tumor volume at the time of measurement by the tumor volume at the time the HIFU treatment was performed. The tumor growth curves of the individual animals were fitted with a monoexponential function ($y = y_0 + A\, e^{Bt}$ for the ablation, hyperthermia plus TSL, ablation plus TSL, and hyp-ab plus TSL treatment or $y = A\, e^{Bt}$ for all other treatment groups), and the tumor tripling time was derived from the fitted equation. An average coefficient of determination (R^2_{adj}) of 0.97 ± 0.04 was obtained, indicating that the data were well fitted using above equations. A survival analysis was carried out, assuming the tumor volume tripling time as the survival endpoint.

For assessment of potential therapy-related toxicity, the body weight of the animals was monitored. The body weight ratio was calculated by dividing the body weight posttreatment through the body weight at treatment.

ACKNOWLEDGMENTS. We thank Iris Verel (Philips Research Eindhoven), Caren van Kammen, Carlijn van Helvert, and Marleen Hendriks (all Maastricht University) for the support with the animal experiments. This research was performed within the framework of the Center for Translational Molecular Medicine (www.ctmm.nl), Volumetric Thermal Ablation Project (Grant 05T-201), and supported by NanoNextNL (FES0901:FES HTSM), the European Union Project SONODRUGS (NMP4-LA-2008-213706), and the European Union Seventh Framework Programme (FP7/2007-2013) under Grant Agreement 603028 (Image-Guided Pancreatic Cancer Therapy Project).

1. Breasted JH (1930) *The Edwin Smith Surgical Papyrus* (Facsimile Plates and Line for Line Hieroglyphic Transliteration) (Univ of Chicago Press, Chicago), Vol 2.
2. Coley WB (1893) The treatment of malignant tumors by repeated inoculations of erysipelas: With a report of ten original cases. *Am J Med Sci* 105:487–511.
3. Singh BB (1991) Hyperthermia: An ancient science in India. *Int J Hyperthermia* 7:1–6.
4. van der Zee J, et al.; Dutch Deep Hyperthermia Group (2000) Comparison of radiotherapy alone with radiotherapy plus hyperthermia in locally advanced pelvic tumours: A prospective, randomised, multicentre trial. *Lancet* 355:1119–1125.
5. Franckena M, et al. (2009) Hyperthermia dose-effect relationship in 420 patients with cervical cancer treated with combined radiotherapy and hyperthermia. *Eur J Cancer* 45:1969–1978.
6. Harima Y, et al. (2001) A randomized clinical trial of radiation therapy versus thermoradiotherapy in stage IIIB cervical carcinoma. *Int J Hyperthermia* 17:97–105.
7. Issels RD, et al.; European Organisation for Research and Treatment of Cancer Soft Tissue and Bone Sarcoma Group (EORTC-STBSG); European Society for Hyperthermic Oncology (ESHO) (2010) Neo-adjuvant chemotherapy alone or with regional hyperthermia for localised high-risk soft-tissue sarcoma: A randomised phase 3 multicentre study. *Lancet Oncol* 11:561–570.
8. Wessalowski R, et al.; MAKEI study group (2013) Regional deep hyperthermia for salvage treatment of children and adolescents with refractory or recurrent non-testicular malignant germ-cell tumours: An open-label, non-randomised, single-institution, phase 2 study. *Lancet Oncol* 14:843–852.
9. Datta NR, Rogers S, Ordóñez SG, Puric E, Bodis S (2016) Hyperthermia and radiotherapy in the management of head and neck cancers: A systematic review and meta-analysis. *Int J Hyperthermia* 32:31–40.
10. Jones EL, et al. (2005) Randomized trial of hyperthermia and radiation for superficial tumors. *J Clin Oncol* 23:3079–3085.
11. Shen H, et al. (2011) The regimen of gemcitabine and cisplatin combined with radio frequency hyperthermia for advanced non-small cell lung cancer: A phase II study. *Int J Hyperthermia* 27:27–32.
12. Yarovoy AA, Magaramov DA, Bulgakova ES (2012) The comparison of ruthenium brachytherapy and simultaneous transpupillary thermotherapy of choroidal melanoma with brachytherapy alone. *Brachytherapy* 11:224–229.
13. Kouloulias V, et al. (2005) Chemoradiotherapy combined with intracavitary hyperthermia for anal cancer: Feasibility and long-term results from a phase II randomized trial. *Am J Clin Oncol* 28:91–99.

14. Colombo R, Salonia A, Leib Z, Pavone-Macaluso M, Engelstein D (2011) Long-term outcomes of a randomized controlled trial comparing thermochemotherapy with mitomycin-C alone as adjuvant treatment for non-muscle-invasive bladder cancer (NMIBC). *BJU Int* 107:912–918.
15. Datta NR, et al. (2015) Local hyperthermia combined with radiotherapy and-/or chemotherapy: Recent advances and promises for the future. *Cancer Treat Rev* 41:742–753.
16. Diederich CJ (2005) Thermal ablation and high-temperature thermal therapy: Overview of technology and clinical implementation. *Int J Hyperthermia* 21:745–753.
17. Hectors SJCG, Jacobs I, Moonen CTW, Strijkers GJ, Nicolay K (2016) MRI methods for the evaluation of high intensity focused ultrasound tumor treatment: Current status and future needs. *Magn Reson Med* 75:302–317.
18. Schmitz AC, et al. (2010) Precise correlation between MRI and histopathology—exploring treatment margins for MRI-guided localized breast cancer therapy. *Radiother Oncol* 97:225–232.
19. Chu KF, Dupuy DE (2014) Thermal ablation of tumours: Biological mechanisms and advances in therapy. *Nat Rev Cancer* 14:199–208.
20. Nakazawa T, et al. (2007) Radiofrequency ablation of hepatocellular carcinoma: Correlation between local tumor progression after ablation and ablative margin. *AJR Am J Roentgenol* 188:480–488.
21. Kim YS, et al. (2010) The minimal ablative margin of radiofrequency ablation of hepatocellular carcinoma (>2 and <5 cm) needed to prevent local tumor progression: 3D quantitative assessment using CT image fusion. *AJR Am J Roentgenol* 195:758–765.
22. Yatvin MB, Weinstein JN, Dennis WH, Blumenthal R (1978) Design of liposomes for enhanced local release of drugs by hyperthermia. *Science* 202:1290–1293.
23. Weinstein JN, Magin RL, Yatvin MB, Zaharko DS (1979) Liposomes and local hyperthermia: Selective delivery of methotrexate to heated tumors. *Science* 204:188–191.
24. Celsion (January 31, 2013) Celsion Announces Results of Phase III HEAT Study of ThermoDox in Primary Liver Cancer. Available at investor.celsion.com/releasedetail.cfm?releaseid=737033. Accessed May 4, 2017.
25. Celsion (August 6, 2015) Celsion Corporation Announces Updated Overall Survival Data from HEAT Study of ThermoDox in Primary Liver Cancer. Available at investor.celsion.com/releasedetail.cfm?ReleaseID=926288. Accessed May 4, 2017.
26. Gasselhuber A, et al. (2010) Mathematical spatio-temporal model of drug delivery from low temperature sensitive liposomes during radiofrequency tumour ablation. *Int J Hyperthermia* 26:499–513.
27. Hijnen NM, et al. (2012) Tumour hyperthermia and ablation in rats using a clinical MR-HIFU system equipped with a dedicated small animal set-up. *Int J Hyperthermia* 28:141–155.
28. Köhler MO, et al. (2009) Volumetric HIFU ablation guided by multiplane MRI thermometry. *AIP Conf Proc* 1113:228–230.
29. Grüll H, Langereis S (2012) Hyperthermia-triggered drug delivery from temperature-sensitive liposomes using MRI-guided high intensity focused ultrasound. *J Control Release* 161:317–327.
30. Staruch R, Chopra R, Hynynen K (2011) Localised drug release using MRI-controlled focused ultrasound hyperthermia. *Int J Hyperthermia* 27:156–171.
31. Staruch RM, Hynynen K, Chopra R (2015) Hyperthermia-mediated doxorubicin release from thermosensitive liposomes using MR-HIFU: Therapeutic effect in rabbit Vx2 tumours. *Int J Hyperthermia* 31:118–133.
32. Kneepkens E, Fernandes A, Nicolay K, Grüll H (2016) Iron(III)-based magnetic resonance-imageable liposomal T1 contrast agent for monitoring temperature-induced image-guided drug delivery. *Invest Radiol* 51:735–745.
33. de Smet M, Heijman E, Langereis S, Hijnen NM, Grüll H (2011) Magnetic resonance imaging of high intensity focused ultrasound mediated drug delivery from temperature-sensitive liposomes: An in vivo proof-of-concept study. *J Control Release* 150:102–110.
34. de Smet M, et al. (2013) Magnetic resonance guided high-intensity focused ultrasound mediated hyperthermia improves the intratumoral distribution of temperature-sensitive liposomal doxorubicin. *Invest Radiol* 48:395–405.
35. Partanen A, et al. (2012) Mild hyperthermia with magnetic resonance-guided high-intensity focused ultrasound for applications in drug delivery. *Int J Hyperthermia* 28: 320–336.
36. Ranjan A, et al. (2012) Image-guided drug delivery with magnetic resonance guided high intensity focused ultrasound and temperature sensitive liposomes in a rabbit Vx2 tumor model. *J Control Release* 158:487–494.
37. Hijnen N, Langereis S, Grüll H (2014) Magnetic resonance guided high-intensity focused ultrasound for image-guided temperature-induced drug delivery. *Adv Drug Deliv Rev* 72:65–81.
38. Peller M, et al. (2016) Surrogate MRI markers for hyperthermia-induced release of doxorubicin from thermosensitive liposomes in tumors. *J Control Release* 237: 138–146.
39. Tagami T, et al. (2011) MRI monitoring of intratumoral drug delivery and prediction of the therapeutic effect with a multifunctional thermosensitive liposome. *Biomaterials* 32:6570–6578.
40. Negussie AH, et al. (2011) Formulation and characterisation of magnetic resonance imageable thermally sensitive liposomes for use with magnetic resonance-guided high intensity focused ultrasound. *Int J Hyperthermia* 27:140–155.
41. de Smet M, et al. (2013) SPECT/CT imaging of temperature-sensitive liposomes for MR-image guided drug delivery with high intensity focused ultrasound. *J Control Release* 169:82–90.
42. Li L, et al. (2014) A novel two-step mild hyperthermia for advanced liposomal chemotherapy. *J Control Release* 174:202–208.
43. Gasselhuber A, et al. (2012) Targeted drug delivery by high intensity focused ultrasound mediated hyperthermia combined with temperature-sensitive liposomes: Computational modelling and preliminary in vivovalidation. *Int J Hyperthermia* 28:337–348.
44. Maeda H (2010) Tumor-selective delivery of macromolecular drugs via the EPR effect: Background and future prospects. *Bioconjug Chem* 21:797–802.
45. Matsumura Y, Maeda H (1986) A new concept for macromolecular therapeutics in cancer chemotherapy: Mechanism of tumoritropic accumulation of proteins and the antitumor agent smancs. *Cancer Res* 46:6387–6392.
46. Lokerse WJM, et al. (2016) Investigation of particle accumulation, chemosensitivity and thermosensitivity for effective solid tumor therapy using thermosensitive liposomes and hyperthermia. *Theranostics* 6:1717–1731.
47. Kong G, Braun RD, Dewhirst MW (2001) Characterization of the effect of hyperthermia on nanoparticle extravasation from tumor vasculature. *Cancer Res* 61: 3027–3032.
48. Li L, et al. (2013) Improved intratumoral nanoparticle extravasation and penetration by mild hyperthermia. *J Control Release* 167:130–137.
49. Dromi S, et al. (2007) Pulsed-high intensity focused ultrasound and low temperature-sensitive liposomes for enhanced targeted drug delivery and antitumor effect. *Clin Cancer Res* 13:2722–2727.
50. Pfizer, Inc. (2014) Pfizer Information leaflet: Doxorubicin hydrochloride. Available at labeling.pfizer.com/ShowLabeling.aspx?id=530#section-1. Accessed May 4, 2017.
51. European Medicines Agency (2017) Summary of product characteristics: Caelyx. Available at www.ema.europa.eu/ema/index.jsp?curl=pages/medicines/human/medicines/000089/human_med_000683.jsp&mid=WC0b01ac058001d124. Accessed May 4, 2017.
52. Manzoor AA, et al. (2012) Overcoming limitations in nanoparticle drug delivery: Triggered, intravascular release to improve drug penetration into tumors. *Cancer Res* 72:5566–5575.
53. Li L, et al. (2013) Mild hyperthermia triggered doxorubicin release from optimized stealth thermosensitive liposomes improves intratumoral drug delivery and efficacy. *J Control Release* 168:142–150.
54. Head HW, et al. (2010) Combination radiofrequency ablation and intravenous radiolabeled liposomal doxorubicin: Imaging and quantification of increased drug delivery to tumors. *Radiology* 255:405–414.
55. Hectors SJCG, et al. (2015) Multiparametric MRI analysis for the evaluation of MR-guided high intensity focused ultrasound tumor treatment. *NMR Biomed* 28:1125–1140.
56. Viglianti BL, et al. (2006) Chemodosimetry of in vivo tumor liposomal drug concentration using MRI. *Magn Reson Med* 56:1011–1018.
57. Hijnen NM, Elevelt A, Grüll H (2013) Stability and trapping of magnetic resonance imaging contrast agents during high-intensity focused ultrasound ablation therapy. *Invest Radiol* 48:517–524.
58. Hectors SJCG, Jacobs I, Strijkers GJ, Nicolay K (2014) Multiparametric MRI analysis for the identification of high intensity focused ultrasound-treated tumor tissue. *PLoS One* 9:e99936.
59. Graham SJ, Stanisz GJ, Kecojevic A, Bronskill MJ, Henkelman RM (1999) Analysis of changes in MR properties of tissues after heat treatment. *Magn Reson Med* 42: 1061–1071.
60. Judson I, et al. (2001) Randomised phase II trial of pegylated liposomal doxorubicin (DOXIL/CAELYX) versus doxorubicin in the treatment of advanced or metastatic soft tissue sarcoma: A study by the EORTC Soft Tissue and Bone Sarcoma Group. *Eur J Cancer* 37:870–877.
61. O'Brien MER, et al.; CAELYX Breast Cancer Study Group (2004) Reduced cardiotoxicity and comparable efficacy in a phase III trial of pegylated liposomal doxorubicin HCl (CAELYX/Doxil) versus conventional doxorubicin for first-line treatment of metastatic breast cancer. *Ann Oncol* 15:440–449.
62. Harris L, et al.; TLC D-99 Study Group (2002) Liposome-encapsulated doxorubicin compared with conventional doxorubicin in a randomized multicenter trial as first-line therapy of metastatic breast carcinoma. *Cancer* 94:25–36.
63. Matteucci ML, et al. (2000) Hyperthermia increases accumulation of technetium-99m-labeled liposomes in feline sarcomas. *Clin Cancer Res* 6:3748–3755.
64. Kheirolomoom A, et al. (2013) Complete regression of local cancer using temperature-sensitive liposomes combined with ultrasound-mediated hyperthermia. *J Control Release* 172:266–273.
65. Morita K, Zywietz F, Kakinuma K, Tanaka R, Katoh M (2008) Efficacy of doxorubicin thermosensitive liposomes (40 ° C) and local hyperthermia on rat rhabdomyosarcoma. 20:365–372.
66. Tillander M, et al. (2016) High intensity focused ultrasound induced in vivo large volume hyperthermia under 3D MRI temperature control. *Med Phys* 43:1539.
67. Holbrook AB, et al. (2014) Respiration based steering for high intensity focused ultrasound liver ablation. *Magn Reson Med* 71:797–806.
68. Poon RT, Borys N (2009) Lyso-thermosensitive liposomal doxorubicin: A novel approach to enhance efficacy of thermal ablation of liver cancer. *Expert Opin Pharmacother* 10: 333–343.
69. Wood BJ, et al. (2012) Phase I study of heat-deployed liposomal doxorubicin during radiofrequency ablation for hepatic malignancies. *J Vasc Interv Radiol* 23:248–255.e7.
70. Clinicaltrials.gov (2016) Study of ThermoDox with Standardized Radiofrequency Ablation (RFA) for Treatment of Hepatocellular Carcinoma (HCC) (OPTIMA). Available at https://www.clinicaltrials.gov/ct2/show/NCT02112656. Accessed May 4, 2017.
71. Clinicaltrials.gov (2017) Phase 3 Study of ThermoDox with Radiofrequency Ablation (RFA) in Treatment of Hepatocellular Carcinoma (HCC). Available at https://clinicaltrials.gov/ct2/show/NCT00617981. Accessed May 4, 2017.
72. Hak S, et al. (2009) A high relaxivity Gd(III)DOTA-DSPE-based liposomal contrast agent for magnetic resonance imaging. *Eur J Pharm Biopharm* 72:397–404.
73. Dubois LJ, et al. (2011) Preclinical evaluation and validation of [^{18}F]HX4, a promising hypoxia marker for PET imaging. *Proc Natl Acad Sci USA* 108:14620–14625.
74. National Research Council (2011) *Guide for the Care and Use of Laboratory Animals* (National Academies Press, Washington, DC), 8th Ed.
75. Shin W, Gu H, Yang Y (2009) Fast high-resolution T1 mapping using inversion-recovery Look-Locker echo-planar imaging at steady state: Optimization for accuracy and reliability. *Magn Reson Med* 61:899–906.